An Efficient Photocatalyst Structure: TiO2(B) Nanofibers with a Shell of Anatase Nanocrystals

ARTICLE *in* JOURNAL OF THE AMERICAN CHEMICAL SOCIETY · NOVEMBER 2009

Impact Factor: 12.11 · DOI: 10.1021/ja906774k · Source: PubMed

8 AUTHORS, INCLUDING:

Dongjiang Yang
Queensland University of Technology
80 PUBLICATIONS **1,209** CITATIONS
SEE PROFILE

Hongwei Liu
University of Sydney
124 PUBLICATIONS **2,292** CITATIONS
SEE PROFILE

Xuebin Ke
Queensland University of Technology
33 PUBLICATIONS **1,036** CITATIONS
SEE PROFILE

H. Y. Zhu
Queensland University of Technology
189 PUBLICATIONS **7,408** CITATIONS
SEE PROFILE

J|A|C|S
ARTICLES

Published on Web 11/13/2009

An Efficient Photocatalyst Structure: TiO_2(B) Nanofibers with a Shell of Anatase Nanocrystals

Dongjiang Yang,[†] Hongwei Liu,[†] Zhanfeng Zheng,[†] Yong Yuan,[†] Jin-cai Zhao,[‡] Eric R. Waclawik,[†] Xuebin Ke,[†] and Huaiyong Zhu*,[†]

School of Physical and Chemical Sciences, Queensland University of Technology, Brisbane, Qld 4001, Australia, and Institute of Chemistry, The Chinese Academy of Science, Beijing 100080, China

Received August 10, 2009; E-mail: hy.zhu@qut.edu.au

Abstract: A new efficient photocatalyst structure, a shell of anatase nanocrystals on the fibril core of a single TiO_2(B) crystal, was obtained via two consecutive partial phase transition processes. In the first stage of the process, titanate nanofibers reacted with dilute acid solution under moderate hydrothermal conditions, yielding the anatase nanocrystals on the fiber. In the subsequent heating process, the fibril core of titanate was converted into a TiO_2(B) single crystal while the anatase crystals in the shell remained unchanged. The anatase nanocrystals do not attach to the TiO_2(B) core randomly but coherently with a close crystallographic registry to the core to form a stable phase interface. For instance, (001) planes in anatase and (100) planes of TiO_2(B) join together to form a stable interface. Such a unique structure has several features that enhance the photocatalytic activity of these fibers. First, the differences in the band edges of the two phases promote migration of the photogenerated holes from anatase shell to the TiO_2(B) core. Second, the well-matched phase interfaces allow photogenerated electrons and holes to readily migrate across the interfaces because the holes migrate much faster than excited electrons, more holes than electrons migrate to TiO_2(B) and this reduces the recombination of the photogenerated charges in anatase shell. Third, the surface of the anatase shell has both a strong ability to regenerate surface hydroxyl groups and adsorb O_2, the oxidant of the reaction, to yield reactive hydroxyl radicals ($OH^{\cdot}$) through reaction between photogenerated holes and surface hydroxyl groups. The adsorbed O_2 molecules can capture the excited electrons on the surface, forming reactive O_2^- species. The more reactive species generated on the external surface, the higher the photocatalytic activity will be, and generation of the reactive species also contributes to reducing recombination of the photogenerated charges. Indeed, the mixed-phase nanofibers exhibited superior photocatalytic activity for degradation of sulforhodamine B under UV light to the nanofibers of either pure phase alone or mechanical mixtures of the pure phase nanofibers with a similar phase composition. Finally, the nanofibril morphology has an additional advantage that they can be separated readily after reaction for reuse by sedimentation. This is very important because the high cost for separating the catalyst nanocrystals has seriously impeded the applications of TiO_2 photocatalysts on an industrial scale.

I. Introduction

Titanium dioxide (TiO_2) has been extensively studied as a photocatalyst because of its chemical stability and nontoxicity.[1−4] TiO_2 exists mainly in four polymorphs in nature, anatase (tetragonal, space group $I4_1/amd$), rutile (tetragonal, space group $P4_2/mnm$), brookite (orthorhombic, space group $Pbca$), and TiO_2(B) (monoclinic, space group $C2/m$).[5,6] Generally, the anatase phase of TiO_2 has long been considered the most photoactive of these four phases.[7,8] In comparison to anatase, the rutile phase is generally less active due to a lower surface affinity for many organic compounds[9] and a higher rate of recombination of photogenerated charge pairs.[10] Compared with anatase, fewer studies on the photoactivity of brookite and TiO_2(B) have been reported. In addition to TiO_2 materials of a single crystal phase, photocatalysts composed of mixed TiO_2 phases have attracted significant attention, as they can exhibit much higher catalytic activity than either of the component phases. For instance, the well-known P25 powder of Degussa which consists of ∼20% rutile (a TiO_2 phase with low activity generally) and ∼80% anatase, is an exceptionally good

[†] Queensland University of Technology.
[‡] The Chinese Academy of Science.

(1) Fujishima, A.; Hashimoto, K.; Watanabe, H. TiO_2 Photocatalysis: Fundamentals and Applications; BKC, Inc.: Tokyo, 1999.
(2) Hoffman, M. R.; Martin, S. T.; Choi, W.; Bahnemann, D. W. *Chem. Rev.* **1995**, *95*, 69.
(3) Thompson, T. L.; Yates, J. T. *Chem. Rev.* **2006**, *106*, 4428.
(4) Linsebigler, A. L.; Lu, G. Q.; Yates, J. T. *Chem. Rev.* **1995**, *95*, 735.
(5) Bakardjieva, S.; Stengl, V.; Szatmary, L.; Subrt, J.; Lukac, J.; Murafa, N.; Niznansky, D.; Cizek, K.; Jirkovsky, J.; Petrova, N. *J. Mater. Chem.* **2006**, *16*, 1709.
(6) Penn, R. L.; Banfield, J. F. *Am. Mineral.* **1999**, *84*, 871.
(7) Tanaka, K.; Capule, M. F. V.; Hisanaga, T. *Chem. Phys. Lett.* **1991**, *187*, 73.
(8) Yanagisawa, K.; Ovenstone, J. *J. Phys. Chem. B* **1999**, *103*, 7781.
(9) Brohan, L.; Verbaere, A.; Tournoux, M.; Demazeau, G. *Mater. Res. Bull.* **1982**, *17*, 355.
(10) Armstrong, A. R.; Armstrong, G.; Canales, J.; Bruce, P. G. *Angew. Chem., Int. Ed.* **2004**, *43*, 2286.

photocatlyst.[2,11−13] The principal reason for the high activity of P25 for oxidation of organic compounds is considered to be the difference between the conduction band (CB) edges of the two phases, which is able to promote irreversible charge transfer from one phase to the other. The charge transfer serves to reduce the recombination of photogenerated electrons and holes, resulting in superior photoactivity.[13−16] However, migration of the photogenerated charges through these mixed-phase TiO_2 systems is a much more complicated process than is sometimes assumed in the literature.[13−16] The fate of excited electrons in the phase with the higher CB edge may proceed by three pathways: they may (i) recombine with photogenerated holes, (ii) move irreversibly to the other phase, or (iii) migrate to TiO_2 surface and be captured by oxygen molecules, forming O_2^- species. The last route contributes to photocatalytic reactions for which molecule oxygen is the oxidation agent. Likewise, the photogenerated holes in this phase can also proceed in a similar manner: quenching with the excited electrons, moving to the other phase, and migrating to TiO_2 surface to react with surface hydroxyl groups or water. Most photogenerated excitons recombine, releasing heat.[1−4] There are two factors that strongly influence the charge transfer from the phase possessing the higher conduction band edge to the other phase. The first is the interface structure, which is crucial to the transfer. Dangling bonds, defects, and large crystallographic discrepancies and voids at the interface region may form charge traps and will hinder the transfer. There are few reports on the structure of the interfaces in mixed-phase photocatalysts existing in literature[13−16] because of the difficulty in determining the interface structures. The second factor is the mobility of the photogenerated charges, as the excited electrons migrate much slower than the holes.[17] This factor also affects the migration of the charges to the surface. Furthermore, the pathways are not independent but interrelate each other. For instance, molecular oxygen on TiO_2 surface is able to capture the excited CB electrons through the formation of superoxide ions, which can subsequently transform to other active chemical species,[4,18−22] reducing the recombination of electron−hole pairs.[4]

In principle, the efficient charge separation via irreversible charge transfer, claimed for P25, should be applicable to other systems of mixed TiO_2 phases as long as there is a sufficient difference between the CB edges to cause irreversible charge transfer from one phase to another. However, whether the transfer enhances the activity of a photocatalyst with mixed TiO_2 phases or not may also depend on other structural properties of the catalyst, such as the component phases and their configuration as well as the surface properties of the component phases. It has been reported that the presence of surface hydroxyl groups is indispensable in the generation of reactive hydroxyl radicals ($OH^{\cdot}$) from the direct valence band (VB) holes oxidation.[2,3] These surface OH groups also facilitate adsorption and activation of molecular oxygen.[23,24]

To achieve comprehensive understanding of the performance of mixed TiO_2 phase photocatalysts, the unsolved questions above must be clarified, and this could be important for designing superior photocatalysts and for understanding photocatalysis processes. For instance, the knowledge can be used for develop new mixed-phase photocatalysts with TiO_2 phases other than anatase and rutile.

$TiO_2(B)$, a metastable monoclinic modification of TiO_2, was first synthesized in 1980 by Marchand et al.[25,26] and was first found in nature by Banfield et al.[27] Up to now, limited studies on the photoactivity of pure $TiO_2(B)$[25,28−30] and mixed-phase composites containing anatase and $TiO_2(B)$ have been reported,[31] probably because there are no readily available commercial $TiO_2(B)$ products, and no facile synthesis has been reported. Although the photoactivity of $TiO_2(B)$ solids is generally much lower than that of anatase, the electronic band gap is narrower than that of the anatase.[29,30] There should thus be a difference between the CB edges of the two phases, when the two phase are in connection. The difference can promote charge transfer from one phase to the other, similar to the situation of P25. The interfaces between the two phases function like one-way valves of the photogenerated charges. As the holes migrate much faster than electrons,[17] an increase of the holes in $TiO_2(B)$ and a decrease of holes in anatase are expected under light irradiation. These will reduce recombination of photogenerated electrons and holes in the anatase phase and thus improve the photocatalytic efficiency of this phase. Among numerous synthesis methods for obtaining pure phase $TiO_2(B)$, thermal dehydration of $H_2Ti_3O_7$ is the most feasible because $H_2Ti_3O_7$ nanofibers can be prepared readily by a hydrothermal reaction between NaOH and a titanium compound, even mineral rutile.[32−34] Herein, nanofibril catalysts with a delicate composite structure, in which a $TiO_2(B)$ fiber is anchored with anatase nanocrystals, are developed via two consecutive partial phase transition processes of $H_2Ti_3O_7$ nanofibers. In this composite core−shell fibril structure, the anatase crystals are oriented to form stable interfaces with the $TiO_2(B)$ fibril core. Under UV light, the mixed-phase TiO_2 nanofibers exhibit superior photo-

(11) Bickley, R. I.; Gonzalez-Carreno, T.; Lees, J. S.; Palmisano, L.; Tilley, R. J. D. *J. Solid State Chem.* **1991**, *92*, 178.
(12) Berger, T.; Sterrer, M.; Diwald, O.; Knozinger, E.; Panayotov, D.; Thompson, T. L.; Yates, J. T. *J. Phys. Chem. B* **2005**, *109*, 6061.
(13) Hurum, D. C.; Agrios, A. G.; Gray, K. A.; Rajh, T.; Thurnauer, M. C. *J. Phys. Chem. B* **2003**, *107*, 4545.
(14) Kawahara, T.; Konishi, Y.; Tada, H.; Tohge, N.; Nishii, J.; Ito, S. *Angew. Chem., Int. Ed.* **2002**, *114*, 2935.
(15) Hurum, D. C.; Agrios, A. G.; Crist, S. E.; Gray, K. A.; Rajh, T.; Thurnauer, M. C. *J. Electron Spectrosc. Relat. Phenom.* **2006**, *150*, 155.
(16) Hurum, D. C.; Gray, K. A.; Rajh, T.; Thurnauer, M. C. *J. Phys. Chem. B* **2004**, *108*, 16483.
(17) Enright, B.; Fitzmaurice, D. *J. Phys. Chem.* **1996**, *100*, 1027.
(18) Peiró, A. M.; Colombo, C.; Doyle, Gerry.; Nelson, J.; Mills, A.; Durrant, J. R. *J. Phys. Chem. B* **2006**, *110*, 23255.
(19) Schwitzgebel, J.; Ekerdt, J. G.; Gerischer, H.; Heller, A. *J. Phys. Chem.* **1995**, *99*, 5633.
(20) Ahmed, S.; Fonseca, S. M.; Kemp, T. J.; Unwin, P. R. *J. Phys.Chem. B* **2003**, *107*, 5892.
(21) Henderson, M. A.; Epling, W. S.; Perkins, C. L.; Peden, C. H. F.; Diebold, U. *J. Phys. Chem. B* **1999**, *103*, 5328.
(22) Nakamura, R.; Imanishi, A.; Murakoshi, K.; Nakato, Y. *J. Am. Chem. Soc.* **2003**, *125*, 7443.
(23) Liu, L. M.; McAllister, B.; Ye, H. Q.; Hu, P. *J. Am. Chem. Soc.* **2006**, *128*, 4017.
(24) Henderson, M. A.; Epling, W. S.; Peden, C. H. F.; Perkins, C. L. *J. Phys. Chem. B* **2003**, *107*, 534.
(25) Marchiand, R.; Brohan, L.; Tournoux, M. *Mater. Res. Bull.* **1980**, *15*, 1129.
(26) Tournoux, M.; Marchand, R.; Brohan, L. *Prog. Solid State Chem.* **1986**, *17*, 33.
(27) Banfield, J.; Veblen, D.; Smith, D. *Am. Mineral.* **1991**, *76*, 343.
(28) Nuspl, G.; Yoshizawa, K.; Yamabe, T. *J. Mater. Chem.* **1997**, *7*, 2529.
(29) Yin, S.; Fujishiro, Y.; Wu, J.; Aki, M.; Sato, H. *J. Mater. Proc. Technol.* **2003**, *137*, 45.
(30) Yin, S.; Wu, J.; Aki, M.; Sato, H. *Int. J. Inorg. Mater.* **2000**, *2*, 325.
(31) Kuo, H.-L.; Kuo, C.-Y.; Liu, C.-H.; Chao, J.-H.; Lin, C.-H. *Catal. Lett.* **2007**, *113*, 7.
(32) Zhu, H. Y.; Gao, X. P.; Lan, Y.; Song, D. Y.; Xi, Y. X.; Zhao, J. C. *J. Am. Chem. Soc.* **2004**, *126*, 8380.
(33) Lan, Y.; Gao, X. P.; Zhu, H. Y.; Zheng, Z. F.; Yan, T. Y.; Wu, F.; Ringer, S. P.; Song, D. Y. *Adv. Funct. Mater.* **2005**, *15*, 1310.
(34) Zhu, H. Y.; Lan, Y.; Gao, X. P.; Ringer, S. P.; Zheng, Z. F.; Song, D. Y.; J, C.; Zhao, *J. Am. Chem. Soc.* **2005**, *127*, 6730.

Table 1. Physicochemical Properties of the Synthesized TiO_2 Nanofibril Photocatalysts

sample	hydrothermal reaction time (h)	phase composition [anatase/TiO_2(B)][a]	crystallite size (nm)[b]	S_{BET} (m^2/g)
T(B)	0	0/100	TiO_2(B)	27.1
T(AB)_8	8	5/95	10.83	39.7
T(AB)_40	40	34/66	21.68	51.2
T(AB)_49	49	74/26	23.45	53.5
T(AB)_52	53	83/17	24.74	55.0
T(A)	60	100/0	26.72	48.7

[a] The molar ratio of TiO_2(B) to anatase phase was calculated from the intensity ratio ($I_{33.4°}/I_{37.8°}$) of the peak at 33.4° to the peak at 37.8°, which correspond to the (311) plane of TiO_2(B) (JCPDS 74-1940) and the (004) plane of anatase (JCPDS21-1272). [b] Average crystallite size was estimated from XRD line-broadening of anatase at 25.3° by employing the Scherrer equation.

catalytic activity for degradation of the organic dye sulforhodamine B (SRB) compared to P25. We ascribe the high photoactivity to the well-matched interfaces formed between the anatase and TiO_2(B), which acts as a gate that permits only unidirectional migration of photogenerated charges, and the core/shell fiber morphology.

II. Experimental Section

1. Synthesis of Mixed-Phase Fibers. Generally, 6 g of anatase particles (~325 mesh from Aldrich) was mixed with 80 mL of 10 M NaOH.[32−34] The suspensions were sonicated in an ultrasonic bath for 0.5 h and then transferred into an autoclave with a PTFE container inside. The autoclave was maintained at hydrothermal temperature of 180 °C for 48 h. The precipitate (sodium titanate nanofibers) was recovered, washed with distilled water (to remove excess NaOH), exchanged with H^+ (using a 0.1 M HCl solution) to produce $H_2Ti_3O_7$ nanofibers, and washed again with distilled water until pH ~7 was reached. The $H_2Ti_3O_7$ nanofiber product was dried at 80 °C for 12 h. The mixed-phase nanofibers were prepared from the $H_2Ti_3O_7$ nanofibers by two-step treatment, hydrothermal reaction and heating process. In the first step, the $H_2Ti_3O_7$ nanofibers reacted with dilute acid under hydrothermal conditions to form the outer anatase nanocrystal shell. For instance, 0.4 g of $H_2Ti_3O_7$ nanofibers were dispersed in a dilute (0.05 M, 40 mL) HNO_3 acid solution and kept at 383 K for 8, 40, 49, and 52 h, respectively. The contents of anatase phase on the outer surface of the fibers could be controlled by tuning the reaction time of the hydrothermal process. In the second step, the $H_2Ti_3O_7$ nanofibers covered with anatase nanocrystal shell were heated at 723 K to convert the $H_2Ti_3O_7$ phase into the TiO_2(B) phase while the anatase nanocrystal shell remained unchanged. The delicate TiO_2 nanofibers with anatase shell and TiO_2(B) core with different mass ratios of anatase to TiO_2(B) were obtained and labeled as T(AB)_8, T(AB)_40, T(AB)_49, and T(AB)_52 (see Table 1). The numbers in the sample label indicate the duration of the acid reaction under hydrothermal conditions (in hours). For instance, T(AB)_49 is the sample obtained after 49 h of acid reaction. For comparison, pure anatase catalyst, noted as T(A), was prepared by prolonging the hydrothermal reaction time to 60 h and calcining at 723 K; pure TiO_2(B) catalyst, T(B), was synthesized by heating the $H_2Ti_3O_7$ nanofibers at 723 K.

2. Sample Characterization. The TEM study on the fibers was conducted using a Philips CM200 TEM with an accelerating voltage of 200 kV, and a high-resolution TEM (HRTEM) investigation was carried out on a FEI Tecnai F20 operating at 200 kV. XRD patterns of the samples were recorded on a Philips PANalytical X'Pert PRO diffractometer using Cu Kα radiation ($\lambda = 1.5418$ Å) operating at 40 kV and 40 mA with a fixed slit. The Raman spectra of the samples were measured on a Spectra-Physics model 127, the excitation source was He−Ne laser (633 nm), and the resolution was 2 cm^{-1}. To investigate the light absorption and emission behavior of the samples as well as their energy band gap, we measured the diffuse reflectance UV−visible (DR-UV−vis) spectra of the samples on a Varian Cary 5000 spectrometer. The nitrogen sorption isotherms were measured by volumetric method on an automatic adsorption instrument (Micromeritics, Tristar 3000) at liquid nitrogen temperature (77 K). Specific surface area was calculated by the Brunauer−Emmett−Teller (BET) method from the data in a P/P_0 range between 0.05 and 0.2. Electron paramagnetic resonance (EPR) spectra were recorded with a Bruker EPR ELEXSYS 500 spectrometer operating at a frequency of 9.5 GHz in the X-band mode. Measurements were performed with an ER 4131 VT variable-temperature accessory at 135 K. The spectra were acquired when samples within the cavity were illuminated at 135 K by UV light, and an irradiation source (a Quanta-Ray Nd: YAG laser system with a wavelength of 355 nm) was used. FTIR emission spectra (IES) was carried out on a Digilab FTS-60A spectrometer equipped with a TGS detector, which was modified by replacing the IR source with an emission cell (principles of the emission experiment have been published elsewhere[35]). The same amount (in volume) of powders for different samples was loaded on the sample holder to form a uniform thin layer. During the IES measurement, the specimen was heated from 100 to 400 °C and then cooled from 400 to 100 °C on a sample holder at the interval of 50 °C in N_2 flow (15 sccm, deliberately controlled with a flow meter) in an closed but not sealed chamber to remove desorbed species from the specimen. The interval between two scans (while the temperature was raised to the next hold point) was approximately 120 s for the powdered sample to reach temperature equilibrium.

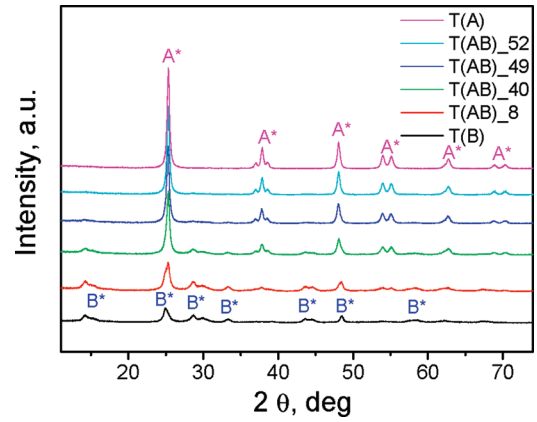

Figure 1. The XRD patterns of the mixed-phase TiO_2 nanofiber photocatalysts.

3. Photocatalytic Activity Test. The UV light source for photoactivity test was six tubular Hg lamps (NEC, FL20SBL) of 20 W, and the peak of the wavelength was at about 350 nm. The catalyst concentration was 0.5 g/L, and the initial concentration (C_0) of the sulforhodamine B (Aldrich) was 1.8×10^{-5} M. At regular irradiation time intervals, the dispersion was sampled, and the specimen was filtered through a Millipore filter (400 nm, Teflon) to remove the catalyst particles prior to the analysis. The filtrate was analyzed by UV−vis spectra (Varian Cary 100 spectrometer) for the absorbance intensity using the reading at 565 nm.

III. Results and Discussion

1. XRD Patterns and Raman Spectra. The XRD patterns of the nanofiber catalysts are shown in Figure 1. Diffraction peaks from both anatase and TiO_2(B) phases were observed in the patterns of different samples T(AB)_8, T(AB)_40, T(AB)_49,

(35) Vittadini, A.; Selloni, A.; Rotzinger, F. P.; Grätzel, M. *Phys. Rev. Lett.* **1998**, *81*, 2954–2957.

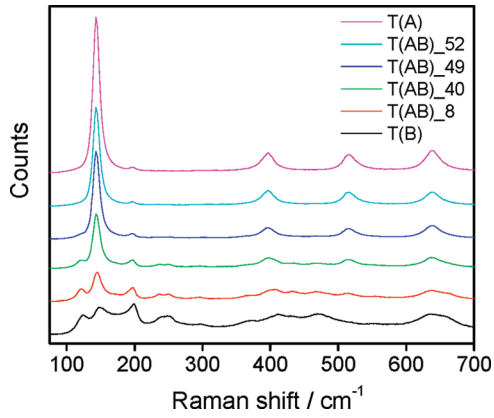

Figure 2. Raman spectra of the mixed-phase TiO_2 nanofiber photocatalysts.

and T(AB)_52, indicating that these fibers possessed a mixed-phase structure. The anatase content was observed to increase gradually with increasing hydrothermal reaction time [from T(AB)_8 to T(AB)_52]. The molar ratio between TiO_2(B) and anatase phase was calculated from the intensity ratio ($I_{33.4°}/I_{37.8°}$) of the peak at 33.4° to the peak at 37.8°, which are reflections from the ($\bar{3}11$) plane of TiO_2(B) (JCPDS 74-1940) and the (004) plane of anatase (JCPDS 21-1272), respectively. The anatase fractions in the above four mixed-phase fibers were 5, 34, 72, and 83%, respectively (Table 1). When the hydrothermal reaction time was prolonged to 60 h, the initial titanate fibers completely converted to anatase [T(A)]. This phase transition regime was also confirmed by analysis of Raman spectra of the samples. As shown in Figure 2, the intensity of the peak at 143 cm^{-1}, which is from anatase lattice, increases gradually with the increase of hydrothermal reaction time [from T(AB)_8 to T(AB)_52]. It also confirms that longer acid reaction duration results in higher anatase content in the products. Other physicochemical properties, such as average anatase crystallite size and specific surface area, are listed in Table 1. It shows that prolonging the hydrothermal reaction yields nanofibers with larger anatase crystallite size and larger specific surface areas. But this effect becomes less important when the reaction time is longer than 40 h. For instance, when the hydrothermal reaction time is between 40 and 60 h, the average anatase crystallite sizes of the outer shells are 21−27 nm, and the specific surface areas of the fibers are 48−55 $m^2\ g^{-1}$. Given the minor difference in the anatase crystallite size and the specific surface area of T(AB)_40, T(AB)_49, T(AB)_52, and T(A), they are not determining factors on photocatalytic activity for these samples in the present study.

2. Morphology. TEM was used to study the structural details of the mixed-phase nanofibers. The result of sample T(AB)_40, as a representative, is given in Figure 3. For comparison, the images of parent $H_2Ti_3O_7$ nanofibers are also presented. As shown in Figure 3a, the sample inherited a fibril morphology from the parent $H_2Ti_3O_7$ nanofibers (Figure 3d). It was observed from the TEM micrograph of a single fiber (Figure 3b) that anatase nanocrystals of 10−20 nm width were coated on the outer surface of the nanofiber. As the electron diffraction (ED) pattern of the single nanofiber further confirmed that the nanofibers were composed of both anatase and TiO_2(B) phases (Figures 3c), the core of nanofibers is TiO_2(B) phase. Such a composite structure provides a large external surface area of the anatase nanocrystals, which have a high photocatalytic activity and can be accessed readily by reactant molecules, thus benefiting the photocatalytic activity. According to the analysis of the ED pattern, the whole TiO_2(B) fibril core is a single crystal, which is expected to provide excellent mechanical properties to the fibers. The parent $H_2Ti_3O_7$ nanofiber has a smooth external surface (Figure 3d) and also consists of a single crystal according to the ED pattern (Figure 3e). Obviously, after the consecutive partial phase transition processes, the single crystal $H_2Ti_3O_7$ nanofiber converted to a composite mixed-phase TiO_2 nanofiber consisting of a single TiO_2(B) crystal core inside a shell of anatase nanocrystals.

3. Photoactivity. The photoactivities of the samples and commercial P25 for degradation of SRB dye are shown in Figure 4a. Clearly, except for sample T(AB)_8, the mixed-phase catalyst's performance was far superior to the pure anatase and TiO_2(B) catalyst, and they were comparable to, or even more active than, P25. Among the mixed-phase fibril catalysts, T(AB)_49 with the anatase/TiO_2(B) phase composition of about 3:1 exhibited the best photocatalytic activity. As mentioned above, the most mixed-phase fibers and the pure anatase catalysts have similar anatase crystal sizes and specific surface areas (Table 1). The high photocatalytic activity of the mixed-phase nanofibers should be attributed to structural factors other than these two. The interfaces between the two phases (phase interfaces) are an important structural component in the mixed-phase nanofibers. Their contribution to the photocatalytic activity was investigated. Mixtures with various mass ratios of TiO_2(B) to anatase were prepared by mechanically mixing nanofibers of pure TiO_2(B) [T(B)] and pure anatase [T(A)], using a pestle and mortar. In Figure 4b, the photocatlytic activities of the mechanical mixtures for photocatalytic degradation of synthetic dye SRB are compared with those of the mixed-phase nanofibers. The percentage of the SRB decomposed after 30 min of UV light irradiation was used for comparing the activities of catalysts. Apparently, the activity of the mechanical mixture increases with the increasing content of the anatase nanofibers, but it was always significantly lower than that of mixed-phase nanofibers with similar phase composition. Given that the nanofibers of the mechanical mixtures separate from each other when dispersed into a solution, a major difference between the mechanical mixtures of the fibers of the pure phases and the nanofibers of the mixed phases is that there are interfaces between the two phases in the later but not in the former. It follows that the superior photocatalytic performance of the mixed-phase fibers is due to the interfaces.

4. Phase Interface. As the phase interfaces have important contribution to the photoactivity, their structures were further investigated. The TEM image and analysis of the corresponding ED pattern show that the anatase crystals attached to the TiO_2(B) fibril cores with a preferred orientation rather than being attached randomly to the core. This means that there are limited ways by which the anatase crystals can attach to the core and thus a definite number of structures of the phase interface.

Figure 5a shows a joint (red rectangle) of anatase nanocrystal and TiO_2(B) phase in a fiber of T(AB)_40 sample. As can be seen, the two phases matched perfectly to form a stable interface (Figure 5b). However, the resolution was not sufficient to provide a measure of the atomic arrangement of the interface. We therefore conducted a fast Fourier transformation (FFT) over the rectangle area marked in Figure 5b to obtain electron diffraction patterns of both anatase and TiO_2(B) from this area. After filtering out noise, which may come from defects and dislocation of atoms, sharp patterns were obtained and converted back to an image by inversing FFT (IFFT). From the IFFT

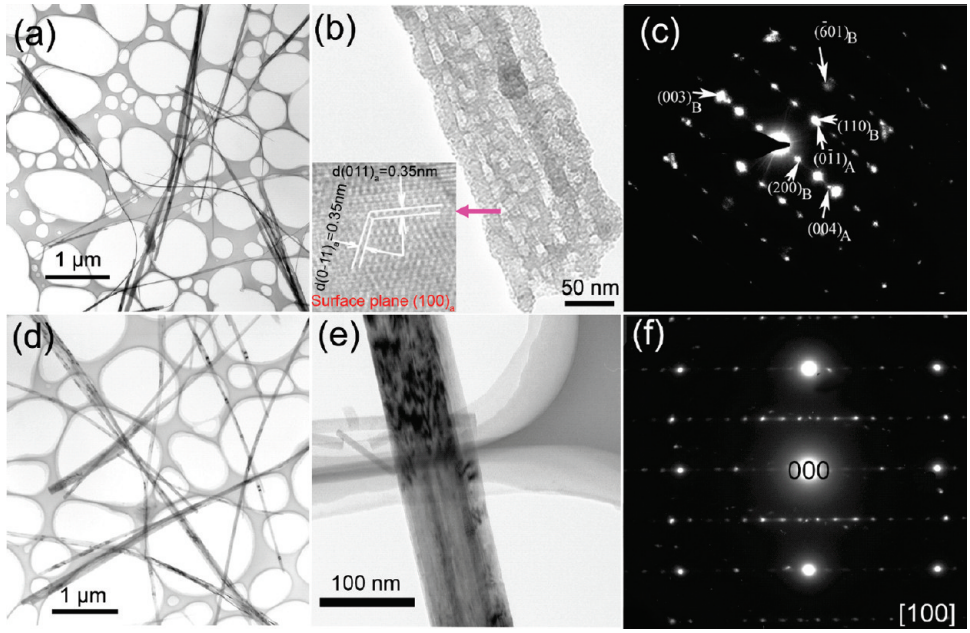

Figure 3. TEM images and electron diffraction patterns of T(AB)_40 (a−c) and parent $H_2Ti_3O_7$ nanofibers (d−f).

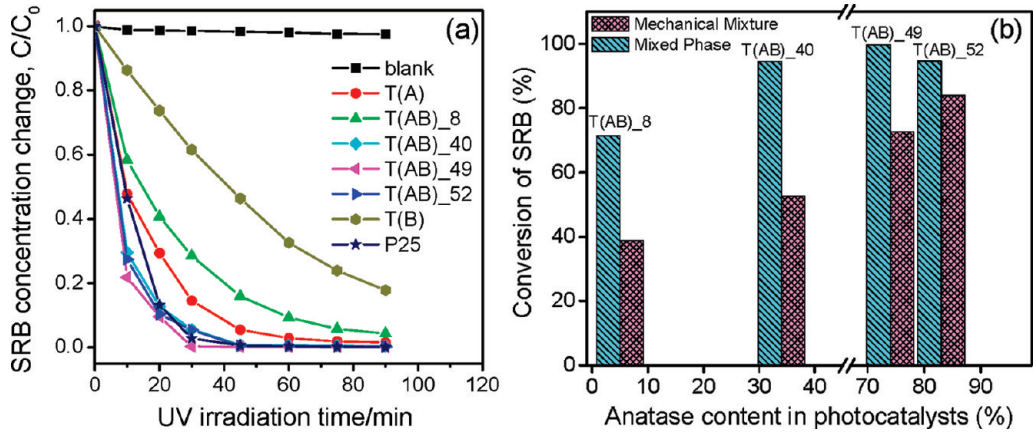

Figure 4. (a) Photocatalytic decomposition of SRB with different fibril TiO_2 photocatalysts under UV irradiation. (b) Comparison of conversion rate for the decomposition of SRB with mechanically mixed TiO_2 photocatalysts. The bars for the mechanical mixture should be for mixed-phase fibers and vice versa.

image (Figure 5c), we could determine the interface: the (001) plane of anatase connects the (100) plane of TiO_2(B), giving the appearance that the (010) planes of anatase crystal extend across the interface and into the TiO_2(B) core. The schematic atomic arrangement of the interface between the two phases was derived on the basis of such crystal orientation and is displayed in Figure 5d.

The atomic arrangement in Figure 5d shows that the engaged crystals are well-matched at the atomic level; such a close crystallographic registry between adjacent crystals is able to minimize the formation of dangling bonds, large crystallographic discrepancies, and voids in the interface region. This atomic arrangement at the crystal interfaces should facilitate interfacial charge transfer in these composites. Obviously, such a structurally stable interface can only form when the engaged crystal planes from two combined crystals possess common crystallographic elements. Therefore, there are a finite number of interfaces that meet this matching requirement in a pair of the engaged crystals.

5. IES Measurements. It is known that water molecules can either dissociate at oxygen vacancies (defects) at the bridging O^{2-} sites on the TiO_2 surface, yielding surface OH groups, or physically adsorb on these sites.[35] These physically adsorbed and dissociated H_2O molecules can be monitored by measuring the infrared (IR) spectra of the samples.[36−39] Also, DFT calculation by Hu et al.[23] showed that molecular O_2 cannot absorb on a perfect TiO_2 surface but instead can only absorb on O-vacancies, while the surface OH groups could facilitate the absorption of molecular O_2 by donating electrons to TiO_2, and these excess electrons are delocalized among Ti (5c) atoms that act as the active sites to absorb molecular O_2. As molecular O_2 is the oxidant for the photocatalytic oxidation, O_2 activation is the key step of the reaction. Thus, the density of surface OH groups and the ability to form the surface OH groups have important influence on the catalytic activity of a sample. In the present study, the IES technique was employed to investigate surface OH groups on different TiO_2 phases. IES spectra of the TiO_2 samples are shown in Figure 6. During the IES measure-

(36) Hadjiivanov, K. I.; Klissurski, D. G. *Chem. Soc. Rev.* **1996**, *25*, 61.
(37) Yates, D. J. C. *J. Phys. Chem.* **1961**, *65*, 746.
(38) Jackson, P.; Parfitt, G. D. *Trans. Faraday Soc.* **1971**, 2469.
(39) Primet, M.; Pichat, P.; Mathieu, M. *J. Phys. Chem.* **1971**, *75*, 1216.

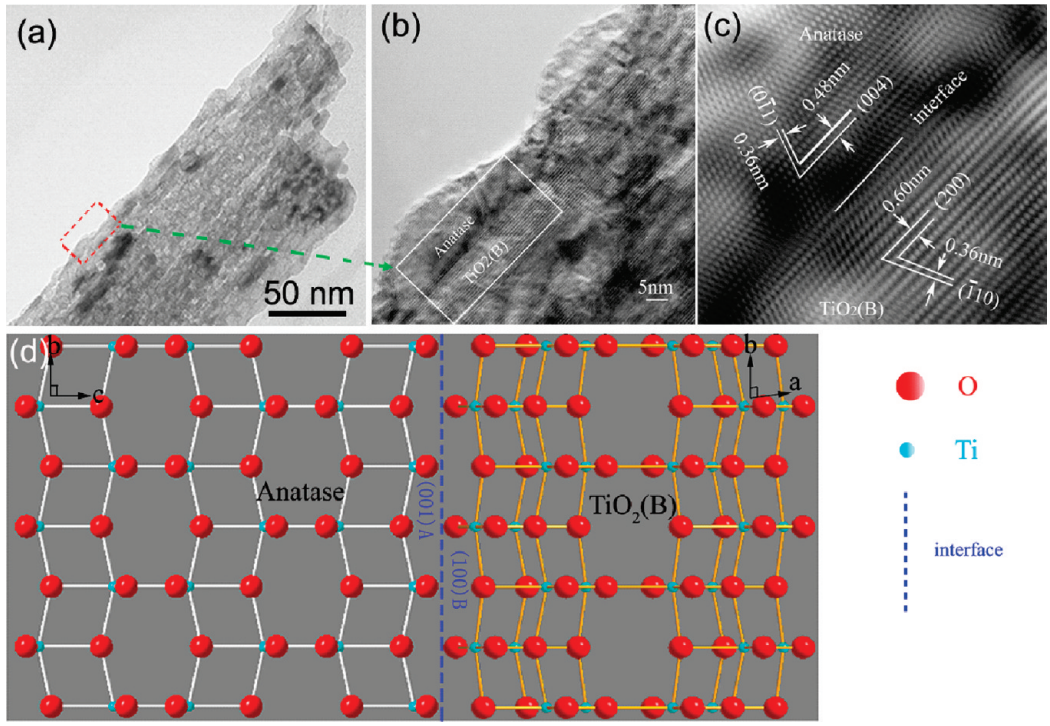

Figure 5. Images of the joint of anatase nanocrystal and TiO_2(B) core in a single T(AB)_40 fiber: (a) TEM images, (b) HRTEM image, (c) inverse fast Fourier transition (IFFT) image of the selected area, and (d) schematic atomic arrangement of the interface between TiO_2(B) and anatase phase.

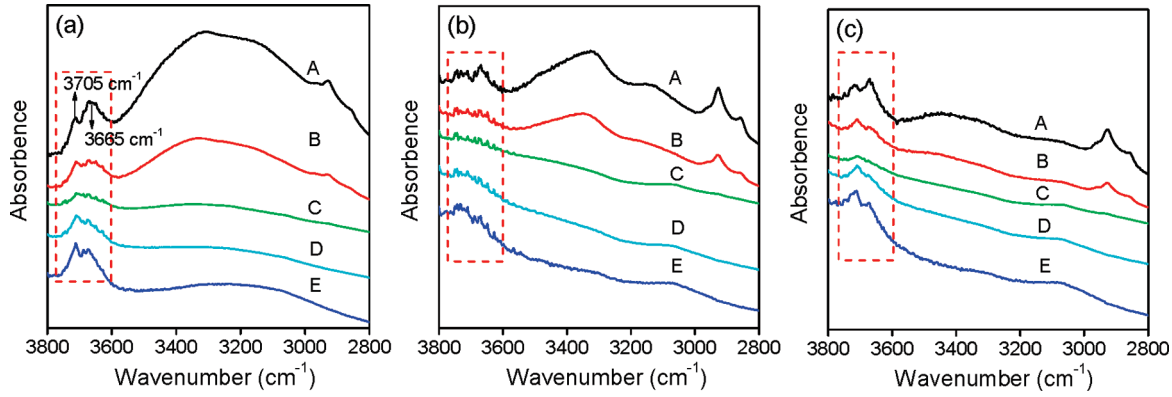

Figure 6. IES spectra of (a) T(A), (b) T(B), and (c) T(AB)_49 samples. Traces A−C were measured at 200, 300, and 400 °C, respectively. Traces D and E were obtained after the temperature was lowered from 400 to 300 and 200 °C, respectively.

ment, the spectra were recorded in situ when the sample was heated on a sample holder from 100 to 400 °C at the interval of 50 °C in a N_2 flow. As can be seen, two OH stretching bands at 3705 and 3665 cm^{-1} were observed for all the samples. The band at 3665 cm^{-1} was assigned to H-bonded (adjacent) OH groups, while the band at 3705 cm^{-1} was assigned to isolated OH groups.[39] The ability of the samples to form the surface OH groups can be derived by comparing the intensity changes of these two bands for different samples when they were heated or cooled down.

For pure anatase nanofibers, the band at 3665 cm^{-1} was more liable to the high temperature and the intensity of the band decreased considerably when the samples were heated from 200 to 400 °C (Figure 6a). When the temperature was lowered gradually, the intensity of the band at 3665 cm^{-1} restored obviously, which means that the anatase surface has a strong ability to regenerate surface OH groups by adsorbing and dissociating water molecules (rehydoxylation). In contrast, the intensity of this band for pure TiO_2(B) nanofibers (Figure 6b) was much lower than that of pure anatase fibers, suggesting that TiO_2(B) nanofibers have a much weaker ability to regenerate surface OH groups compared to anatase fibers. This is an important reason for the lower photocatalytic activity of TiO_2(B) phase, compared with that of anatase phase. As anticipated, the mixed-phase nanofibers have the ability to regenerate surface OH groups better than pure TiO_2(B) nanofibers but weaker than pure anatase nanofibers (Figure 6c). The IES experiment is highly reproducible and reliable. In the IES spectra, the band between 3200 and 3400 cm^{-1} is attributed to the stretching vibration of the water molecules that are H-bonded.[37,38] When the specimen was heated to above 400 °C, the band disappeared, indicating that the absorbed water could be readily removed. Both peaks between 3000 and 2800 cm^{-1} are assigned to the stretching bands of CH_3 of the adsorbed organic solvents, such as CH_3OH.[40] These small organic molecules in air are easily

(40) Chuang, C.-C.; Chen, C.-C.; Lin, J.-L. *J. Phys. Chem. B* **1999**, *103*, 2439.

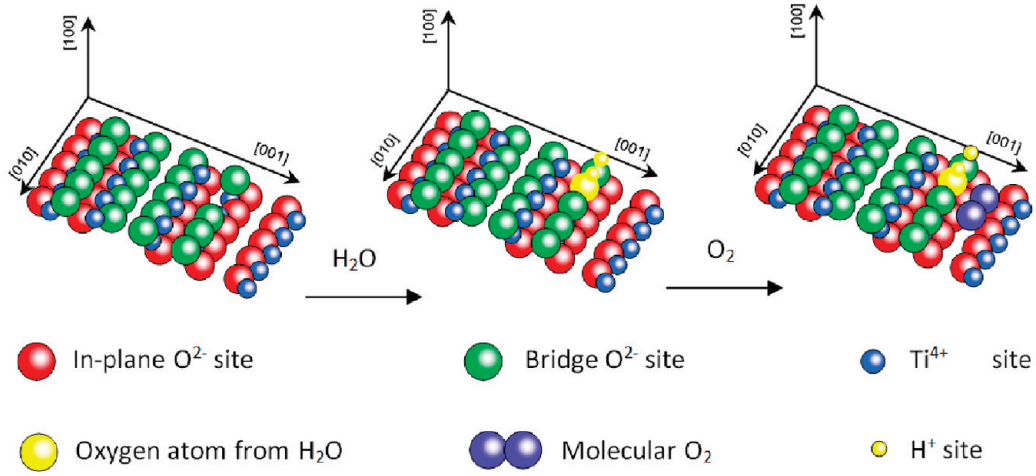

Figure 7. Proposed H_2O and O_2 adsorption process on exposure to the (100) plane in anatase.

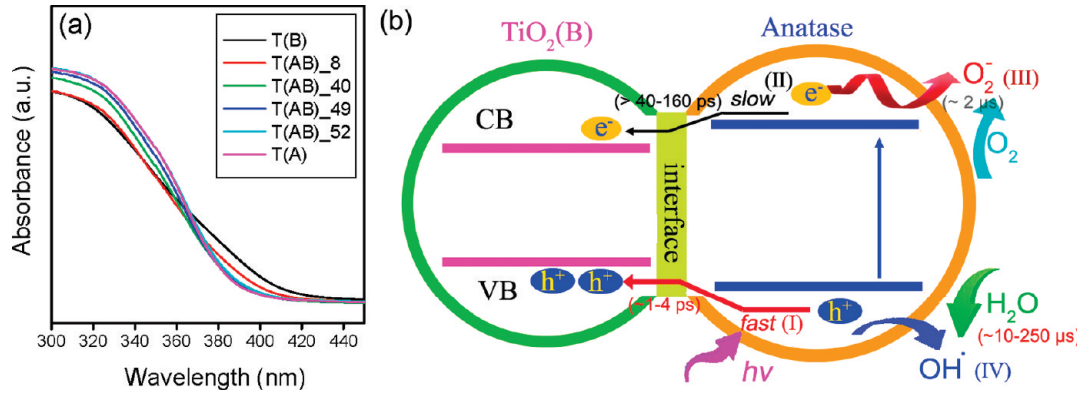

Figure 8. (a) UV−visible diffuse reflectance spectra of the synthesized TiO_2 nanfibril photocatalysts. (b) Possible electron−hole separation mechanism of mixed-phase nanofibers during photocatalysis driven by UV light illumination.

adsorbed on the surface of the TiO_2 nanofibers or clays.[41] When heated to 400 °C, these small organic molecules are removed and the both peaks disappear.

According to the TEM analysis (Figure 3b), the most exposed surface of anatase shell is the (100) plane. Combining literature results with the results in the present study, we can propose a structural model to illustrate the absorption of H_2O and O_2 molecules on the anatase (100) plane, as illustrated in Figure 7. Both the absorption and the activation of molecular O_2 are related to the surface O-vacancy density and distribution. A water molecule can readily dissociate into OH groups at the oxygen vacancies. The OH groups facilitate O_2 adsorption on TiO_2 surface,[23] and the adsorbed O_2 molecules can efficiently capture photogenerated electrons to form active O_2^- species. Bonapasta et al.[42] reported that O_2 molecules could be adsorbed on a (100) anatase surface, introducing an acceptor level in the band gap to entrap photogenerated electrons. Obviously, the mixed-phase nanofibers are apt to form O_2^- species on the exposed external surface shell of anatase crystals. However, the single crystal TiO_2(B) core of the nanofibers cannot contribute to the absorption and the activation of O_2 molecules, as the molecules have little chance to access this phase, and the better ability of anatase surface to absorb and activate O_2 molecules alone cannot explain the superior activity of the mixed-phase nanofibers to the pure anatase nanofibers. As shown in Figure 4b, the activity of the mechanical mixture of the nanofibers of pure TiO_2(B) and pure anatase increases steadily with the increasing content of the anatase nanofibers but is always lower than that of mixed-phase nanofibers with similar phase composition. This superior activity must also involve the transfer of the photogenerated charges between the anatase and TiO_2(B) phase, which is related to the interfaces between the two phases.

6. Proposed Hole Migration Mechanism. Nuspl et al. calculated the electronic structure of TiO_2(B) and concluded that TiO_2(B) is an n-type semiconductor with a band gap of 3−3.22 eV.[20] According to the UV−vis diffusion reflectance (UV−vis DR) spectra of the samples (Figure 8a), we calculated the absorption edge by plotting $[F(R)E]^{1/2}$ against E, where $F(R)$ is the Kubelka−Munk function and E is the photon energy, and extrapolating the straight linear portion of the UV−vis spectra to $[F(R)E]^{1/2} = 0$.[43,44] The band gaps of TiO_2(B) and anatase phase thus obtained are ~3.05 and ~3.19 eV, respectively. This means that when the two phases are in contact there will be a difference between the band edges of the engaged phases. The differences can promote charge transfer from anatase to the other phase, similar to the situation of P25. The well-matched phase interfaces make it possible for the photogenerated charges to

(41) Kloprogge, J. T.; Frost, R. L.; Hickey, L. *Thermochim. Acta* **2000**, *345*, 145.
(42) Bonapasta, A. A.; Filippone, F. *Surf. Sci.* **2005**, *577*, 59.
(43) Koffyberg, F. P.; Dwight, K.; Wold, A. *Solid State Commun.* **1979**, *30*, 433.
(44) Kim, Y. I.; Atherton, S. J.; Brigham, E. S.; Mallouk, T. E. *J. Phys. Chem. B* **1993**, *97*, 11802.

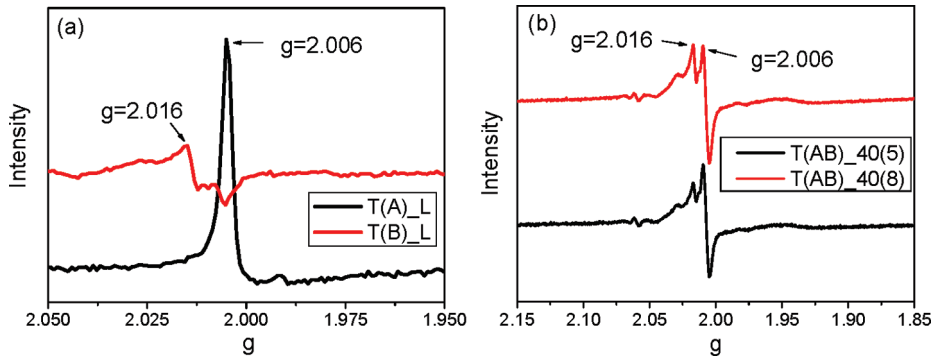

Figure 9. (a) EPR spectra of pure anatase [T(A)_L] and TiO_2(B) [T(B)_L] nanofibers after 20 min of UV exposure (355 nm, 100 W). (b) EPR spectra of mixed-phase T(AB)_40 nanofiber after 5 and 8 min of UV illumination. All the samples are measured at 135 K.

migrate from anatase to TiO_2(B) and function like one-way valves, permitting the charges to migrate from anatase to TiO_2(B) only.

When the UV light irradiates the external anatase phase shell, the photogenerated charges from the valence band (VB) can pass through the interface and migrate to the VB in the TiO_2(B) phase. The hole diffusivity D of anatase TiO_2 at room temperature is known to be about 4×10^{-5} m^2/s.[17] It takes about 1−4 ps for holes in the crystals of the anatase shell to migrate to the phase interface between anatase and TiO_2(B) or to the external surfaces. The time (τ) is estimated by the equation below:

$$\tau = r_0^2/(\pi^2 D)$$

where r_0 is the radius of the particle. The size ($2r_0$) of anatase nanocrystals is between 10 and 20 nm. In contrast, diffusion of the electrons is calculated to be lower than 1×10^{-6} m^2/s, because the effective mass of the electrons ($m_e^* > 10\ m_e$) is much larger than that of holes ($m_h^* = 0.8m_e$) in anatase TiO_2. This means the times required for electrons to migrate to the same destinations in the same anatase crystals are 40 times longer (>40−160 ps) than those for holes. Therefore, as shown in Figure 8b, the photogenerated holes (process I) can migrate more promptly to the adjacent TiO_2(B) phase than the photogenerated electrons (process II). The overall outcome for the interphase charge transfer from the shell of anatase to the core of TiO_2(B) should be that the holes move from anatase to TiO_2(B), and this has been detected by electron paramagnetic resonance (EPR). The EPR spectra of the nanofibrous catalysts T(A), T(B), and T(AB)_40 are displayed in Figure 9. These spectra were collected at 135 K, which can be used to observe the signal of the holes in the catalysts.[45] This signal is also called single electron trapped oxygen vacancy in the literature. As shown in Figure 9a, a hole signal peak at $g = 2.006$ was found in the spectrum of the pure anatase nanofibers after UV irradiation; the hole signal peak of the pure TiO_2(B) nanofibers was located at $g = 2.016$. For the mixed-phase nanofibers, T(AB)_40, both peaks at $g = 2.006$ and $g = 2.016$ were observed after the sample was exposed to the UV irradiation for 5 min [Figure 9b, T(AB)_40(5)]. More interestingly, when the UV irradiation time was extended to 8 min, the peak at $g = 2.016$ was enhanced, indicating that an increase in hole concentration in TiO_2(B) occurred, while a slight decrease of peak at $g = 2.006$ was detected, meaning that the holes in the anatase phase were reduced. The EPR analysis suggests that the net charge transfer between the two phases is that holes in the valence band of anatase phase transfer to the valence band of TiO_2(B).

The O_2 molecules adsorbed on the anatase surface can capture photogenerated electrons that migrate to the surface (process III in Figure 8b). This process reduces the recombination of the photogenerated charges and efficiency of the photocatalysis, although the process takes a relatively long time (~2 μs), compared to interphase charge transfer (several to over one hundred picoseconds). Similarly, holes migrating to the surface of the anatase shell can react directly with surface hydroxyl groups to generate reactive hydroxyl radicals ($OH^{\bullet}$).[23] This process (process IV in Figure 8b) is slower (~10−250 μs), compared to the process in which adsorbed oxygen molecules capture electrons. As a consequence, more holes than excited electrons are left in anatase crystals under light irradiation, and this concentration gradient of charges between the two phases is another factor driving more holes to TiO_2(B).

UV irradiation can penetrate the anatase shell and be absorbed by TiO_2(B), but the excited electrons in the TiO_2(B) core cannot migrate to the anatase shell because the CB edge of TiO_2(B) is lower than that of anatase. The holes in TiO_2(B) cannot migrate to anatase shell, either, for the similar reasons. Besides, it is hard for the photogenerated charges in the core of TiO_2(B) to react with surface species because the TiO_2(B) surface is not exposed (covered by anatase shell). Therefore, the sole fate of the photogenerated charges in the TiO_2(B) core is recombination.

The analysis reveals that the configuration of the component phases in the mixed-phase catalysts is important. It is rational that the shell exposed to reactants should form by the phase having better ability to adsorb and activate O_2, the oxidant of the reaction, and to generate reactive $OH^{\cdot}$. According to IES analysis, the surface of anatase has better ability to generate the surface OH groups that facilitate O_2 adsorption. The adsorbed O_2 molecules capture the excited electrons, forming active O_2^- species on the anatase surface. TiO_2(B) surface has a poorer ability to regenerate surface OH groups, so TiO_2(B) is not suitable to form the shell. However, the single crystal TiO_2(B) core can provide good mechanical strength for the nanofibers and accept the holes that migrated from the anatase shell. The later property reduces the charge recombination in the shell. As most of the photogenerated charges end up recombining, moderate reduction of the recombination is able to considerably enhance the photocatalytic efficiency. Also, the stable interfaces formed from well-matched lattice planes of the two phases are crucial for the charge separation and stability of the photocatalyst. Holes can pass across the stable interfaces

(45) Zhang, S. L.; Li, W.; Jin, Z. S.; Yang, J. J.; Zhang, J. W.; Du, Z. L.; Zhang, Z. J. *J. Solid State Chem.* **2004**, *177*, 1365.

with the least difficulty. With the above three unique features, the mixed-phase nanofibers exhibited superior photocatalytic activity over pure anatase and TiO_2(B). The close crystallographic registry between the anatase crystals in the shell and TiO_2(B) core assures high structural stability and long operation of the photocatalysts.

IV. Conclusion

In summary, mixed-phase nanofibers with a shell of anatase nanocrystals on the fibril core of a single TiO_2(B) crystal were prepared from $H_2Ti_3O_7$ nanofibers by consecutive partial phase transition processes: hydrothermal reaction and subsequent heating process. In these fibers the single crystal TiO_2(B) cores provided a superior mechanical property, and anatase nanocrystals coated on TiO_2(B) cores with a preferred orientation form well-matched and stable phase interfaces. The differences in the band edges of the two phases can promote migration of the photogenerated holes from anatase nanocrystals in the outer shell to the TiO_2(B) core; meanwhile, the external surface of anatase shell has a strong ability to adsorb O_2, the oxidant of the reaction. The photogenerated electrons in the shell can be entrapped by the adsorbed O_2 molecules. Both interphase transfer of the holes and the electron capturing on the surface contribute to reducing recombination of the photogenerated charges. As anatase surface has the strong ability to regenerate surface hydroxyl groups, the reactive hydroxyl radicals ($OH^{\bullet}$) can be yielded on the external surface of anatase shell by the reaction of holes and surface hydroxyl groups. The formed reactive species are located on the external surface of the anatase shell and are easily accessed by the reactants, assuring high photocatalytic activity. The well-matched phase interfaces facilitate effective migration of the photogenerated charges across the interfaces, and this migration can reduce charge recombination and enhances photoactivity. The matched interfaces also ensure the high structural stability of the photocatalysts and long operation life. Furthermore, these nanofiber photocatalysts possess specific surface areas similar to P25 powder, but their fibril morphology allow them to be readily separated from fluid after use by filtration or sedimentation. For example, the mixed-phase nanofibers can sediment from an aqueous suspension in less than 1 h. However, the aqueous suspensions of a commercial P25 remain turbid after 24 h of sedimentation. This is very important, because the high cost for separating the catalyst nanocrystals has seriously impeded the applications of TiO_2 photocatalysts on an industrial scale.

Acknowledgment. This research is supported by the Australian Research Council (ARC).

JA906774K